University Library

MINERVA ACCESS

A gateway to Melbourne's research publications

Minerva Access is the Institutional Repository of The University of Melbourne

Author/s:
Bianchini, F;Wu, WLK;Ade, PAR;Anderson, AJ;Austermann, JE;Avva, JS;Beall, JA;Bender, AN;Benson, BA;Bleem, LE;Carlstrom, JE;Chang, CL;Chaubal, P;Chiang, HC;Citron, R;Moran, CC;Crawford, TM;Crites, AT;de Haan, T;Dobbs, MA;Everett, W;Gallicchio, J;George, EM;Gilbert, A;Gupta, N;Halverson, NW;Harrington, N;Henning, JW;Hilton, GC;Holder, GP;Holzapfel, WL;Hrubes, JD;Huang, N;Hubmayr, J;Irwin, KD;Knox, L;Lee, AT;Li, D;Lowitz, A;Manzotti, A;McMahon, JJ;Meyer, SS;Millea, M;Mocanu, LM;Montgomery, J;Nadolski, A;Natoli, T;Nibarger, JP;Noble, G;Novosad, V;Omori, Y;Padin, S;Patil, S;Pryke, C;Reichardt, CL;Ruhl, JE;Saliwanchik, BR;Sayre, JT;Schaffer, KK;Sievers, C;Simard, G;Smecher, G;Stark, AA;Story, KT;Tucker, C;Vanderlinde, K;Veach, T;Vieira, JD;Wang, G;Whitehorn, N;Yefremenko, V

Title:
Constraints on Cosmological Parameters from the 500 deg(2) SPTPOL Lensing Power Spectrum

Date:
2020-01-16

Citation:
Bianchini, F., Wu, W. L. K., Ade, P. A. R., Anderson, A. J., Austermann, J. E., Avva, J. S., Beall, J. A., Bender, A. N., Benson, B. A., Bleem, L. E., Carlstrom, J. E., Chang, C. L., Chaubal, P., Chiang, H. C., Citron, R., Moran, C. C., Crawford, T. M., Crites, A. T., de Haan, T. ,... Yefremenko, V. (2020). Constraints on Cosmological Parameters from the 500 deg(2) SPTPOL Lensing Power Spectrum. Astrophysical Journal, 888 (2), https://doi.org/10.3847/1538-4357/ab6082.

Persistent Link:
https://hdl.handle.net/11343/251354

Draft version November 18, 2020
Typeset using LaTeX **twocolumn** style in AASTeX62

Constraints on Cosmological Parameters from the 500 deg^2 SPTpol Lensing Power Spectrum

F. Bianchini,[1] W. L. K. Wu,[2] P. A. R. Ade,[3] A. J. Anderson,[4] J. E. Austermann,[5,6] J. S. Avva,[7] J. A. Beall,[5] A. N. Bender,[8,2] B. A. Benson,[4,2,9] L. E. Bleem,[8,2] J. E. Carlstrom,[2,10,8,9,11] C. L. Chang,[2,8,9] P. Chaubal,[1] H. C. Chiang,[12,13] R. Citron,[14] C. Corbett Moran,[15] T. M. Crawford,[2,9] A. T. Crites,[2,9,16] T. de Haan,[7,17] M. A. Dobbs,[12,18] W. Everett,[19] J. Gallicchio,[2,20] E. M. George,[21,7] A. Gilbert,[12] N. Gupta,[1] N. W. Halverson,[19,6] N. Harrington,[7] J. W. Henning,[8,2] G. C. Hilton,[5] G. P. Holder,[22,23,18] W. L. Holzapfel,[7] J. D. Hrubes,[14] N. Huang,[7] J. Hubmayr,[5] K. D. Irwin,[24,25] L. Knox,[26] A. T. Lee,[7,17] D. Li,[5,24] A. Lowitz,[9] A. Manzotti,[2,27] J. J. McMahon,[28] S. S. Meyer,[2,10,9,11] M. Millea,[7] L. M. Mocanu,[2,9] J. Montgomery,[12] A. Nadolski,[22,23] T. Natoli,[9,2,29] J. P. Nibarger,[5] G. Noble,[12] V. Novosad,[30] Y. Omori,[31] S. Padin,[2,9,16] S. Patil,[1] C. Pryke,[32] C. L. Reichardt,[1] J. E. Ruhl,[33] B. R. Saliwanchik,[33,34] J.T. Sayre,[19,6] K. K. Schaffer,[2,11,35] C. Sievers,[14] G. Simard,[12] G. Smecher,[12,36] A. A. Stark,[37] K. T. Story,[31,25] C. Tucker,[3] K. Vanderlinde,[29,38] T. Veach,[39] J. D. Vieira,[22,23] G. Wang,[8] N. Whitehorn,[40] and V. Yefremenko[8]

[1] *School of Physics, University of Melbourne, Parkville, VIC 3010, Australia*
[2] *Kavli Institute for Cosmological Physics, University of Chicago, 5640 South Ellis Avenue, Chicago, IL, USA 60637*
[3] *Cardiff University, Cardiff CF10 3XQ, United Kingdom*
[4] *Fermi National Accelerator Laboratory, MS209, P.O. Box 500, Batavia, IL 60510*
[5] *NIST Quantum Devices Group, 325 Broadway Mailcode 817.03, Boulder, CO, USA 80305*
[6] *Department of Physics, University of Colorado, Boulder, CO, USA 80309*
[7] *Department of Physics, University of California, Berkeley, CA, USA 94720*
[8] *High Energy Physics Division, Argonne National Laboratory, 9700 S. Cass Avenue, Argonne, IL, USA 60439*
[9] *Department of Astronomy and Astrophysics, University of Chicago, 5640 South Ellis Avenue, Chicago, IL, USA 60637*
[10] *Department of Physics, University of Chicago, 5640 South Ellis Avenue, Chicago, IL, USA 60637*
[11] *Enrico Fermi Institute, University of Chicago, 5640 South Ellis Avenue, Chicago, IL, USA 60637*
[12] *Department of Physics, McGill University, 3600 Rue University, Montreal, Quebec H3A 2T8, Canada*
[13] *School of Mathematics, Statistics & Computer Science, University of KwaZulu-Natal, Durban, South Africa*
[14] *University of Chicago, 5640 South Ellis Avenue, Chicago, IL, USA 60637*
[15] *TAPIR, Walter Burke Institute for Theoretical Physics, California Institute of Technology, 1200 E California Blvd, Pasadena, CA, USA 91125*
[16] *California Institute of Technology, MS 249-17, 1216 E. California Blvd., Pasadena, CA, USA 91125*
[17] *Physics Division, Lawrence Berkeley National Laboratory, Berkeley, CA, USA 94720*
[18] *Canadian Institute for Advanced Research, CIFAR Program in Gravity and the Extreme Universe, Toronto, ON, M5G 1Z8, Canada*
[19] *Department of Astrophysical and Planetary Sciences, University of Colorado, Boulder, CO, USA 80309*
[20] *Harvey Mudd College, 301 Platt Blvd., Claremont, CA 91711*
[21] *European Southern Observatory, Karl-Schwarzschild-Str. 2, 85748 Garching bei München, Germany*
[22] *Astronomy Department, University of Illinois at Urbana-Champaign, 1002 W. Green Street, Urbana, IL 61801, USA*
[23] *Department of Physics, University of Illinois Urbana-Champaign, 1110 W. Green Street, Urbana, IL 61801, USA*
[24] *SLAC National Accelerator Laboratory, 2575 Sand Hill Road, Menlo Park, CA 94025*
[25] *Dept. of Physics, Stanford University, 382 Via Pueblo Mall, Stanford, CA 94305*
[26] *Department of Physics, University of California, One Shields Avenue, Davis, CA, USA 95616*
[27] *Institut d'Astrophysique de Paris, 98 bis boulevard Arago, 75014 Paris, France*
[28] *Department of Physics, University of Michigan, 450 Church Street, Ann Arbor, MI, USA 48109*
[29] *Dunlap Institute for Astronomy & Astrophysics, University of Toronto, 50 St George St, Toronto, ON, M5S 3H4, Canada*
[30] *Materials Sciences Division, Argonne National Laboratory, 9700 S. Cass Avenue, Argonne, IL, USA 60439*
[31] *Kavli Institute for Particle Astrophysics and Cosmology, Stanford University, 452 Lomita Mall, Stanford, CA 94305*
[32] *School of Physics and Astronomy, University of Minnesota, 116 Church Street S.E. Minneapolis, MN, USA 55455*
[33] *Physics Department, Center for Education and Research in Cosmology and Astrophysics, Case Western Reserve University, Cleveland, OH, USA 44106*
[34] *Department of Physics, Yale University, P.O. Box 208120, New Haven, CT 06520-8120*
[35] *Liberal Arts Department, School of the Art Institute of Chicago, 112 S Michigan Ave, Chicago, IL, USA 60603*
[36] *Three-Speed Logic, Inc., Vancouver, B.C., V6A 2J8, Canada*
[37] *Harvard-Smithsonian Center for Astrophysics, 60 Garden Street, Cambridge, MA, USA 02138*
[38] *Department of Astronomy & Astrophysics, University of Toronto, 50 St George St, Toronto, ON, M5S 3H4, Canada*
[39] *Department of Astronomy, University of Maryland College Park, MD, USA 20742*

[40] *Department of Physics and Astronomy, University of California, Los Angeles, CA, USA 90095*

ABSTRACT

We present cosmological constraints based on the cosmic microwave background (CMB) lensing potential power spectrum measurement from the recent 500 deg^2 SPTpol survey, the most precise CMB lensing measurement from the ground to date. We fit a flat ΛCDM model to the reconstructed lensing power spectrum alone and in addition with other data sets: baryon acoustic oscillations (BAO) as well as primary CMB spectra from *Planck* and SPTpol. The cosmological constraints based on SPTpol and *Planck* lensing band powers are in good agreement when analysed alone and in combination with *Planck* full-sky primary CMB data. With weak priors on the baryon density and other parameters, the SPTpol CMB lensing data alone provide a 4% constraint on $\sigma_8\Omega_m^{0.25} = 0.593 \pm 0.025$. Jointly fitting with BAO data, we find $\sigma_8 = 0.779 \pm 0.023$, $\Omega_m = 0.368^{+0.032}_{-0.037}$, and $H_0 = 72.0^{+2.1}_{-2.5}\,\mathrm{km\,s^{-1}\,Mpc^{-1}}$, up to $2\,\sigma$ away from the central values preferred by *Planck* lensing + BAO. However, we recover good agreement between SPTpol and *Planck* when restricting the analysis to similar scales. We also consider single-parameter extensions to the flat ΛCDM model. The SPTpol lensing spectrum constrains the spatial curvature to be $\Omega_K = -0.0007 \pm 0.0025$ and the sum of the neutrino masses to be $\sum m_\nu < 0.23$ eV at 95% C.L. (with *Planck* primary CMB and BAO data), in good agreement with the *Planck* lensing results. With the differences in the S/N of the lensing modes and the angular scales covered in the lensing spectra, this analysis represents an important independent check on the full-sky *Planck* lensing measurement.

Keywords: cosmic background radiation - cosmological parameters - gravitational lensing

1. INTRODUCTION

Measurements of the gravitational lensing of the cosmic microwave background (CMB) by large-scale structure provide a unique observational probe of the geometry of the universe and the growth of structure at high redshifts. As light travels from the last-scattering surface to us, the paths of the photons are bent by the gravitational potential of matter. These deflections are related to the gradient of the gravitational potential and can be used to reconstruct the gravitational potential integrated along the line of sight (Lewis & Challinor 2006). Gravitational lensing of the CMB also provides a powerful tool for constraining neutrino masses, since massive neutrinos suppress structure growth (e.g., Lesgourgues & Pastor 2006; Abazajian et al. 2015). CMB lensing has been measured by a number of experiments using both temperature and polarization data (e.g., Das et al. 2011; van Engelen et al. 2012; Planck Collaboration XVII 2013; POLARBEAR Collaboration 2014; Story et al. 2015; Planck Collaboration et al. 2016c; Keck Array et al. 2016; Sherwin et al. 2017; Omori et al. 2017; Planck Collaboration et al. 2018b; Wu et al. 2019). The most precise lensing amplitude measurement to date comes from *Planck*, which measures the overall lensing amplitude at $40\,\sigma$ (Planck Collaboration et al. 2018b).

Intriguingly, there is a modest level of discordance between the primary CMB power spectra from *Planck* and other cosmological probes within the ΛCDM model. Relevant to the case of lensing, the amplitude of density fluctuations σ_8 deduced from galaxy cluster counts and cosmic shear measurements is slightly lower than the value suggested by primary CMB *Planck* data (e.g., Hildebrandt et al. 2017; Abbott et al. 2018; Bocquet et al. 2019; Hikage et al. 2019; Zubeldia & Challinor 2019; Joudaki et al. 2019). Tensions within the *Planck* dataset are also emerging, for example the amount of lensing inferred from the smoothing of the acoustic peaks in the *Planck* CMB power spectra is larger than the one directly measured through the CMB lensing potential power spectrum (Planck Collaboration et al. 2018a). Whether these tensions have their origins in unaccounted for systematics, new physics, or are simply statistical fluctuations is not yet clear and more detailed analyses are needed in order to shed light on these discrepancies.

One way to probe if these apparent tensions are caused by systematics is to use measurements from independent experiments. In this work, we infer cosmological parameters using the high-S/N lensing power spectrum measurement from the 500 deg^2 SPTpol survey (Wu et al. 2019, hereafter W19), currently the most precise CMB lensing measurement from the ground. While measured over only 1% of the sky, the SPTpol lensing amplitude uncertainty is only twice as large as the uncertainty of the *Planck* lensing measurement from 67% of the sky. Thus the SPTpol lensing power spectrum provides a chance to test for consistency between CMB

lensing measurements performed over different fractions of the sky and angular scales. In particular, the SPTpol lensing power spectrum complements the *Planck* lensing measurements by extending the measurement to smaller angular scales. If the two lensing measurements are consistent, their combination has the potential to improve our cosmological model constraints.

In this work, we explore the cosmological implications of the high-significance measurement of the lensing angular power spectrum from W19. Within the ΛCDM model, we begin by comparing cosmological parameters inferred from the SPTpol lensing measurements against those from *Planck* and optical surveys. We then contrast parameters from lensing measurements and primary CMB measurements. After that, we look at what these lensing measurements tell us about the curvature of the universe and the sum of the neutrino masses, as well as other model extensions using a suite of Monte Carlo Markov chains. As in W19, we take the best-fit ΛCDM model for the PlanckTT + lowP + lensing dataset in Planck Collaboration et al. (2016b) to be our fiducial model.

This paper is organized as follows. We outline the principles of CMB lensing and how the lensing potential can be reconstructed in Sec. 2. In Sec. 3, we explore cosmological parameters constraints from the lensing data in different models. Finally, we draw our conclusions in Sec. 4.

2. LENSING RECONSTRUCTION FRAMEWORK

In this section we briefly review the physics of CMB lensing, sketch the lensing reconstruction pipeline steps in the context of SPTpol, and describe the CMB lensing likelihood modelling. For a thorough description of the SPTpol lensing reconstruction analysis, we refer the reader to W19.

2.1. *Basics of CMB lensing*

During their journey from the last-scattering surface to us, CMB photons are deflected by the gradients of gravitational potentials associated with the large-scale structure (LSS) (Blanchard & Schneider 1987; Bernardeau 1997; Lewis & Challinor 2006). As a result, the unlensed CMB temperature $T(\hat{\mathbf{n}})$ and polarization $[Q \pm iU](\hat{\mathbf{n}})$ anisotropies are remapped according to:

$$\tilde{X}(\hat{\mathbf{n}}) = X(\hat{\mathbf{n}} + \mathbf{d}(\hat{\mathbf{n}})), \tag{1}$$

where $X(\hat{\mathbf{n}})$ denotes either the temperature or polarization fluctuations in a given direction of the sky $\hat{\mathbf{n}}$, and the tilde indicates the lensed quantities. At lowest order, the deflection field $\mathbf{d}(\hat{\mathbf{n}})$ can be written as the angular gradient of the Weyl gravitational potential Ψ projected along the line-of-sight, $\mathbf{d}(\hat{\mathbf{n}}) = \nabla\phi(\hat{\mathbf{n}})$, where we have introduced the CMB lensing potential ϕ:

$$\phi(\hat{\mathbf{n}}) = -2\int_0^{\chi_{\rm CMB}} d\chi \frac{f_K(\chi_{\rm CMB}-\chi)}{f_K(\chi_{\rm CMB})f_K(\chi)}\Psi(\chi\hat{\mathbf{n}}, \eta_0-\chi). \tag{2}$$

Here, χ is the comoving distance (with $\chi_{\rm CMB} \approx 14000$ Mpc denoting the distance to the last scattering surface), f_K is the angular-diameter distance, and $\eta_0 - \chi$ is the conformal time. The divergence of the deflection field gives the lensing convergence $\kappa = -\frac{1}{2}\nabla^2\phi$, that quantifies the amount of local (de)magnification of the CMB fluctuations.

Eq. 2 tells us that CMB lensing probes both the geometry and the growth of structure of the universe and as such, precise measurements of its power spectrum can break the geometrical degeneracy affecting the primary CMB (Stompor & Efstathiou 1999) and tighten constraints on the sum of neutrino masses $\sum m_\nu$ as well as on the amplitude of density fluctuations σ_8 (Smith et al. 2009).

2.2. *Lensing extraction with quadratic estimators*

Lensing correlates previously independent CMB temperature and polarization modes between different angular scales on the sky. This lensing-induced correlation is the basis for lensing quadratic estimators, which reconstruct the lensing potential ϕ by examining the correlation between CMB Fourier modes (Zaldarriaga & Seljak 1999; Hu & Okamoto 2002).

The formally optimal estimator (at lowest order in ϕ) has the following form

$$\bar{\phi}^{XY}_{\mathbf{L}} = \int d^2\boldsymbol{\ell}\, W^{XY}_{\boldsymbol{\ell},\boldsymbol{\ell}-\mathbf{L}} \bar{X}_{\boldsymbol{\ell}} \bar{Y}^*_{\boldsymbol{\ell}-\mathbf{L}}, \tag{3}$$

where $\bar{X}$ and $\bar{Y}$ are the filtered T, E, or B fields, and $W^{XY}_{\boldsymbol{\ell},\boldsymbol{\ell}-\mathbf{L}}$ is a weight function (unique to the XY pair, see Hu & Okamoto 2002 for the exact expressions). We recall that in the W19 lensing analysis only CMB modes with $|\boldsymbol{\ell}_x| > 100$ and $|\boldsymbol{\ell}| < 3000$ are used, to account for the impact of time-stream filtering and mitigate foreground contamination. The input CMB maps are filtered with an inverse-variance (C^{-1}) filter to down-weight noisy modes and to increase the sensitivity to lensing. In addition, the unlensed CMB spectra in the weights $W^{XY}_{\boldsymbol{\ell},\boldsymbol{\ell}-\mathbf{L}}$ are replaced with the lensed ones to cancel higher-order biases (Hanson et al. 2011).

The lensing potential $\bar{\phi}^{XY}_{\mathbf{L}}$ measured with Eq. 3 is a biased estimate of the true lensing potential $\phi^{XY}_{\mathbf{L}}$:

$$\bar{\phi}^{XY}_{\mathbf{L}} = \mathcal{R}^{XY}_{\mathbf{L}} \phi^{XY}_{\mathbf{L}}, \tag{4}$$

where $\mathcal{R}_{\mathbf{L}}^{XY}$ is a response function that normalizes the estimator. As discussed in W19, the response function adopted in this analysis is first calculated analytically and then corrected perturbatively with simulations, $\mathcal{R}_{\mathbf{L}}^{XY} = \mathcal{R}_{\mathbf{L}}^{XY,\mathrm{Analytic}}\mathcal{R}_{\mathbf{L}}^{XY,\mathrm{MC}}$. To illustrate the cosmological dependence of this response function, which will be relevant to calculate the corrections to the lensing likelihood in Sec. 2.4, we explicitly write down the analytical response function in the case of an isotropic filter:

$$\mathcal{R}_{\mathbf{L}}^{XY,\mathrm{Analytic}} = \int d^2\boldsymbol{\ell}\, W^{XY}_{\boldsymbol{\ell},\boldsymbol{\ell}-\mathbf{L}} W^{XY}_{\boldsymbol{\ell},\boldsymbol{\ell}-\mathbf{L}} \mathcal{F}^X_{\boldsymbol{\ell}}\, \mathcal{F}^Y_{\boldsymbol{\ell}-\mathbf{L}}, \quad (5)$$

where $\mathcal{F}^X_\ell = \left(C^{XX}_\ell + N^{XX}_\ell\right)^{-1}$. Note that both the filters $\mathcal{F}_\ell$ and the weight functions $W_{\ell,\ell-L}$ are calculated assuming a fiducial cosmology.

Anisotropic features such as inhomogeneous noise and coupling of modes due to masking introduce spurious signals that mimic the effects of lensing. To circumvent this, we remove a mean-field correction $\bar{\phi}^{XY,\mathrm{MF}}_{\mathbf{L}}$ estimated by averaging $\bar{\phi}$ reconstructed from many input lensed CMB simulations. The final estimate of the lensing potential is

$$\hat{\phi}^{XY}_{\mathbf{L}} = \frac{1}{\mathcal{R}^{XY}_{\mathbf{L}}}\left(\bar{\phi}^{XY}_{\mathbf{L}} - \bar{\phi}^{XY,\mathrm{MF}}_{\mathbf{L}}\right). \quad (6)$$

Finally, the different lensing estimators $XY \in \{TT, TE, TB, EE, EB, ET, BT, BE\}$ are combined into a minimum-variance (MV) estimate using

$$\hat{\phi}^{\mathrm{MV}}_{\mathbf{L}} = \frac{1}{\mathcal{R}^{\mathrm{MC}}_{\mathbf{L}}} \frac{\sum_{XY} \bar{\phi}^{XY}_{\mathbf{L}} - \bar{\phi}^{XY,\mathrm{MF}}_{\mathbf{L}}}{\sum_{XY} \mathcal{R}^{XY,\mathrm{Analytic}}_{\mathbf{L}}}. \quad (7)$$

2.3. *Power spectrum estimation*

Cosmological inference is carried out by comparing the measured CMB lensing power spectrum to the theoretical expectations over the parameter space. After obtaining the unbiased lensing potential $\hat{\phi}$, the raw CMB lensing potential power spectrum $C_L^{\hat{\phi}^{XY}\hat{\phi}^{ZW}}$ is measured by forming cross- spectra of $\hat{\phi}^{XY}_{\mathbf{L}}$ and $\hat{\phi}^{ZW}_{\mathbf{L}}$. The resulting power spectrum is a biased estimate of the true CMB lensing power spectrum. In W19, four sources of biases are corrected for (Hu & Okamoto 2002; Kesden et al. 2003; Hanson et al. 2011):

$$\hat{C}^{\phi\phi}_L = f_{\mathrm{PS}}\left[C_L^{\hat{\phi}\hat{\phi}} - N_L^{(0),RD} - N_L^{(1)}\right] - \Delta C_L^{\phi\phi,\mathrm{FG}}. \quad (8)$$

$N_L^{(0)}$ is the disconnected (Gaussian) bias term that arises from chance correlations in the CMB, noise, and foregrounds. We estimate it with the realization-dependent method described in Namikawa et al. (2013) that reduces the covariance between lensing band powers and eliminates the dependency on the fiducial cosmology at linear order. Secondary contractions of the connected 4-point function source an additional bias term, known as $N^{(1)}$, that depends linearly on the true CMB lensing potential power spectrum and hence, on the cosmological parameters. In the flat-sky limit, and assuming an isotropic filtering, it can be evaluated as (Kesden et al. 2003; Planck Collaboration et al. 2016c)

$$\begin{aligned} N_L^{(1)} =& \frac{1}{\mathcal{R}_L^{XZ}\mathcal{R}_L^{CD}} \int \frac{d^2\boldsymbol{\ell}_1}{(2\pi)^2}\frac{d^2\boldsymbol{\ell}'_1}{(2\pi)^2} \\ &\times \mathcal{F}^X_{\ell_1}\mathcal{F}^Z_{\ell_2}\mathcal{F}^C_{\ell'_1}\mathcal{F}^D_{\ell'_2} W^{ZD}_{-\boldsymbol{\ell}_2,\boldsymbol{\ell}'_2} W^{ZD}_{-\boldsymbol{\ell}_2,\boldsymbol{\ell}'_2} \\ &\times \Big[C^{\phi\phi}_{|\boldsymbol{\ell}_1-\boldsymbol{\ell}'_1|} W^{XC}_{-\boldsymbol{\ell}_1,\boldsymbol{\ell}'_1} W^{ZD}_{-\boldsymbol{\ell}_2,\boldsymbol{\ell}'_2} \\ &+ C^{\phi\phi}_{|\boldsymbol{\ell}_1-\boldsymbol{\ell}'_2|} W^{XD}_{-\boldsymbol{\ell}_1,\boldsymbol{\ell}'_2} W^{ZC}_{-\boldsymbol{\ell}_2,\boldsymbol{\ell}'_1}\Big], \end{aligned} \quad (9)$$

where $\boldsymbol{\ell}_1 + \boldsymbol{\ell}_2 = \boldsymbol{\ell}'_1 + \boldsymbol{\ell}'_2 = \mathbf{L}$. In W19, this bias term is estimated using simulations, as done in Story et al. (2015).

Foreground emission can introduce biases in the reconstructed lensing map and the lensing power spectrum, especially if correlated with the LSS. In particular, thermal Sunyaev-Zel'dovich (tSZ) effect and cosmic infrared background (CIB) emission can leak into the reconstructed lensing map correlating with the lensing potential. In addition, tSZ and CIB have trispectra that can leak into the CMB lensing spectrum through the 4-point function of the temperature map. Adopting the bias estimates from van Engelen et al. (2014), we remove a foreground bias term $\Delta C_L^{\phi\phi,\mathrm{FG}}$ from the temperature components of the MV spectrum that include tSZ trispectra, CIB trispectra, $\mathrm{tSZ}^2 - \phi$ and $\mathrm{CIB}^2 - \phi$ contributions.

Higher order biases, like $N_L^{(2)}$ are cancelled by the use of lensed CMB spectra in the lensing weights $W_{\ell,\ell-L}$ (Hanson et al. 2011), while biases induced by the non-Gaussianity of the LSS or by the post-Born corrections are negligible at the current S/N (e.g., Pratten & Lewis 2016; Böhm et al. 2016; Beck et al. 2018).

Any non-idealities not captured by the lensing reconstruction analysis might result in discrepancies between the input theory and the recovered amplitude in simulations. We refer to this residual bias as "Monte Carlo bias" and, in our analysis, we find that the main source of this bias is higher-order coupling generated by the presence of the point-source mask, and we rescale the measured lensing power spectrum by a multiplicative correction f_{PS} of order 5% to account for this effect.

Finally, the lensing bandpower covariance is estimated using $N_s = 400$ Monte Carlo sky realizations that

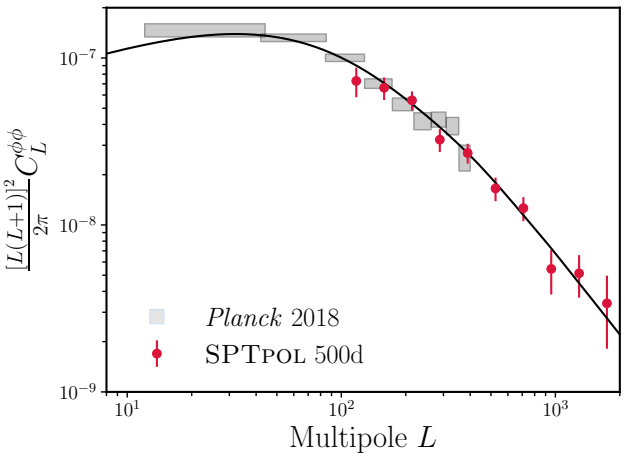


Figure 1. CMB lensing potential power spectrum measurements from SPTpol 500d (Wu et al. 2019, red circles) and from *Planck* 2018 (Planck Collaboration et al. 2018b, grey boxes). The black solid line is the lensing spectrum from the best-fit ΛCDM model to the 2015 PlanckTT + lowP + lensing dataset.

have been fully processed through the lensing analysis pipeline. Specifically, the input CMB maps are passed through a mock observing pipeline that uses the pointing information to produce mock time-ordered data from these simulated skies for each SPT detector, filters those data in the same fashion as the real data, and generates maps using the inverse-noise weights from the real data.

The final CMB lensing band powers used for the cosmological analysis presented in this paper are shown by the red circles in Fig. 1, together with the 2018 *Planck* $C_L^{\phi\phi}$ measurement.

2.4. *CMB lensing likelihood*

We approximate the lensing log-likelihood as Gaussian in the band powers of the estimated lensing power spectrum:

$$-2\ln\mathcal{L}_\phi(\mathbf{\Theta}) = \sum_{ij}\left[\hat{C}^{\phi\phi}_{L^i_\mathrm{b}} - C^{\phi\phi,\mathrm{th}}_{L^i_\mathrm{b}}(\mathbf{\Theta})\right]\mathbb{C}^{-1}_{L^i_\mathrm{b}L^j_\mathrm{b}}\left[\hat{C}^{\phi\phi}_{L^j_\mathrm{b}} - C^{\phi\phi,\mathrm{th}}_{L^j_\mathrm{b}}(\mathbf{\Theta})\right], \tag{10}$$

where $C^{\phi\phi,\mathrm{th}}_{L^i_\mathrm{b}}(\mathbf{\Theta})$ is the binned theory spectrum at the position $\mathbf{\Theta}$ in the parameter space. In Eq. 10 we ignore the correlations between the 2- and 4-point functions since these have been shown to be negligible at current sensitivities (Schmittfull et al. 2013; Peloton et al. 2017). In practice, this means that when combining the CMB power spectra from *Planck* with SPTpol lensing, we simply multiply their respective likelihoods. The covariance matrix $\mathbb{C}^{-1}_{L^i_\mathrm{b}L^j_\mathrm{b}}$ is calculated using Monte Carlo simulations and includes small off-diagonal elements. When inverting the covariance matrix, we neglect the correction from Hartlap et al. (2007) as this is only a $\approx 2-3\%$ effect. For completeness, we also point out that we do not inflate our covariance matrix by a $\approx 4\%$ factor to account for the Monte Carlo uncertainties arising from using a finite number of simulations to estimate the mean-field and the noise biases (Planck Collaboration et al. 2018b).

The fiducial cosmology assumed in the lensing reconstruction affects the estimated lensing band powers. The underlying cosmological parameters do not only enter Eq. 10 through the theoretical lensing power spectrum $C_L^{\phi\phi,\mathrm{th}}(\mathbf{\Theta})$, but also indirectly through the calculation of the response functions $\mathcal{R}_L$ and the $N^{(1)}$ bias. For a given pair of quadratic estimators x and y, the corrected theory lensing power spectrum can be written as

$$C_L^{\phi\phi,\mathrm{th}}|_{\mathbf{\Theta}} = \frac{(\mathcal{R}^x_L\mathcal{R}^y_L)|_{\mathbf{\Theta}}}{(\mathcal{R}^x_L\mathcal{R}^y_L)|_\mathrm{fid}} C_L^{\phi\phi}\big|_{\mathbf{\Theta}} + N_L^{(1)xy}\big|_{\mathbf{\Theta}} - N_L^{(1)xy}\big|_\mathrm{fid}. \tag{11}$$

Evaluating these quantities at each point in the parameter space is computationally unfeasible, therefore we follow the approach of Planck Collaboration et al. (2016c); Sherwin et al. (2017); Simard et al. (2018) and perturbatively correct the theory spectrum for changes due to the parameter deviations from the fiducial cosmology. For such small deviations, we can Taylor-expand the response function and the $N_L^{(1)}$ bias around the fiducial cosmology and obtain:[1]

$$\begin{aligned} C_L^{\phi\phi,\mathrm{th}}|_{\mathbf{\Theta}} &\approx \frac{\partial\ln(\mathcal{R}^x_L\mathcal{R}^y_L)}{\partial C^j_{\ell'}}\left(C^j_{\ell'}|_{\mathbf{\Theta}} - C^j_{\ell'}|_\mathrm{fid}\right)C^{\phi\phi}_{\ell'}|_\mathrm{fid} \\ &\quad + \frac{\partial N_L^{(1)xy}}{\partial C^{\phi\phi}_{L'}}\left(C^{\phi\phi}_{L'}|_{\mathbf{\Theta}} - C^{\phi\phi}_{L'}|_\mathrm{fid}\right) \\ &= C_L^{\phi\phi}\big|_{\mathbf{\Theta}} + M^a_{LL'}\left(C^a_{L'}|_{\mathbf{\Theta}} - C^a_{L'}|_\mathrm{fid}\right) \end{aligned} \tag{12}$$

where summation over repeated indices is implied, j sums over the CMB power spectra TT, TE, and EE, while a also sums over $\phi\phi$ in addition to TT, TE, and EE. The correction matrices $M^a_{LL'}$ can then be pre-computed for the fiducial model and binned. We make use of the publicly available `quicklens`[2] and `lensingbiases`[3] packages to calculate the derivative

[1] We neglect the dependence of the $N_L^{(1)}$ bias on the CMB power spectra. Also note that we use isotropic approximations to model both the response function and the $N_L^{(1)}$ bias.

[2] Available at https://github.com/dhanson/quicklens.

[3] Available at https://github.com/JulienPeloton/lensingbiases

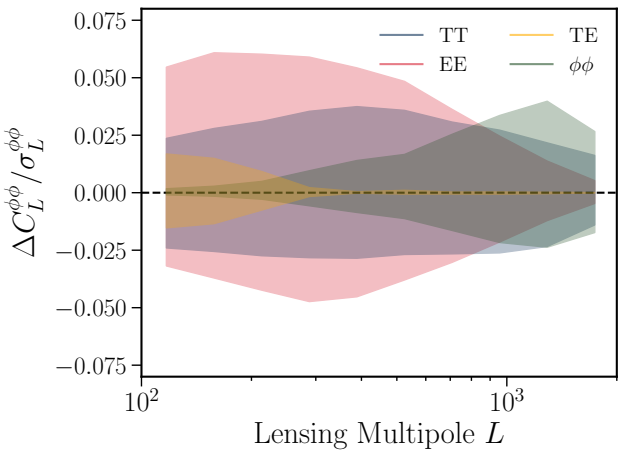


Figure 2. Ratio of the lensing likelihood corrections, $\Delta C_L^{\phi\phi} = M^a_{LL'}\,(C^a_{L'}|_{\boldsymbol{\Theta}} - C^a_{L'}|_{\rm fid})$, to the SPTpol lensing band powers uncertainties $\sigma_L^{\phi\phi}$ for the CMB power spectra $TT/TE/EE$ and $\phi\phi$ corrections (blue, yellow, red, and cyan bands respectively). The different bands contain the 68% of the correction distributions evaluated for points $\boldsymbol{\Theta}$ in the parameter space randomly drawn from the PlanckTT + lowP + lensing cosmology chains from Planck Collaboration et al. (2016b).

with respect to the response function and the $N_L^{(1)}$ bias, respectively. Finally, for the MV CMB lensing power spectrum, we coadd the different xy linear corrections according to the MV weights, as done for the real data. To give a sense of the magnitude and the spectral dependence of the different lensing corrections, we show their breakdown in Fig. 2, evaluated for 100 points in the parameter space randomly drawn from the *Planck* chains corresponding to our fiducial cosmology.

3. COSMOLOGICAL PARAMETER CONSTRAINTS

In this section we investigate the constraining power of the SPTpol lensing dataset on cosmology and compare to *Planck* lensing constraints.

3.1. *Cosmological inference framework*

Our reference cosmological model is a spatially flat ΛCDM model with purely adiabatic scalar primordial fluctuations and a single family of massive neutrinos with total mass $\sum m_\nu = 60$ meV. This baseline model is described by a set of six parameters: the physical baryon density $\Omega_b h^2$, the physical cold dark matter density $\Omega_c h^2$, the (approximated) angular size of the sound horizon at recombination $\theta_{\rm MC}$, the optical depth at reionization τ, the amplitude A_s and spectral index n_s of primordial scalar fluctuations calculated at a pivot scale of $k = 0.05$ Mpc^{-1}. We will also quote parameters derived from these six parameters, such as the total matter density Ω_m, the Hubble constant H_0, and the amplitude of the matter power spectrum expressed in terms of σ_8, the rms density fluctuations within a sphere of radius 8 h^{-1} Mpc. We calculate the lensed CMB and CMB lensing potential power spectra with the `camb`[4] Boltzmann code (Lewis et al. 2000), while the parameter posteriors are sampled with the Markov Chain Monte Carlo (MCMC) `CosmoMC`[5] code (Lewis & Bridle 2002).

In the following we combine the likelihoods associated to five different datasets: i) the 2015 PlanckTT and lowP primary CMB likelihoods (Planck Collaboration et al. 2016a); ii) the 2018 *Planck* CMB lensing likelihood (Planck Collaboration et al. 2018b); iii) the SPTpol CMB lensing likelihood[6]; iv) the SPTpol $TEEE$ likelihood (Henning et al. 2018); v) baryonic acoustic oscillation (BAO) likelihoods from BOSS DR12, SDSS MGS, and 6dFGS galaxy surveys data (Beutler et al. 2011; Ross et al. 2015; Alam et al. 2017).

We do not use the latest *Planck* 2018 primary CMB data because the *Planck* 2018 likelihoods were only publicly released when the analysis and preparation of this manuscript were near completion. Since the main aim of this work is to compare the constraining power of the SPTpol and *Planck* lensing datasets, this does not represent an issue as long as we combine them with the same primary CMB datasets. For completeness, we recall that the main differences between the 2015 and 2018 *Planck* releases are an improved processing of the low-ℓ HFI polarization data and the inclusion of polarization corrections in the high-ℓ likelihood (not used here), whose principal effect is to lower the central value and tighten the uncertainty by a factor of 2 on τ. Consequently, the $A_s e^{-2\tau}$ degeneracy causes a 1σ decrease of $\ln(10^{10}A_s)$ and a $\approx 0.5\sigma$ increase of $\Omega_c h^2$.

3.2. *Constraints from CMB lensing alone*

We start by showing the constraints on the baseline ΛCDM model using only CMB lensing measurements.

[4] Available at https://camb.info (August 2017 version). The small-scale nonlinear matter power spectrum and its effect on the CMB lensing quantities are calculated with the `HMcode` of Mead et al. (2015). The effect of the non-linear matter power spectrum modelling uncertainties on the estimated cosmological parameters has been shown to be negligible by Planck Collaboration et al. (2018b), who compared constraints obtained adopting both the Takahashi et al. (2012) and Mead et al. (2015) versions of the `halofit` model. The impact of modelling differences is found to be negligible even when considering the full multipole range $8 \leq L \leq 2048$.

[5] Available at https://cosmologist.info/cosmomc/ (July 2018 version)

[6] Details on how to install and use the SPTpol CMB lensing likelihood and dataset are available at https://pole.uchicago.edu/public/data/lensing19/.

Table 1. Summary of the priors imposed on each cosmological parameter in this work, when considering either lensing-only datasets or also including primary CMB measurements. Parameters that are fixed are reported by a single number. $\mathcal{U}(a,b)$ denotes a uniform distribution between $[a,b]$, while $\mathcal{N}(\mu,\sigma^2)$ indicates a Gaussian distribution with mean μ and variance σ^2.

Parameter	Lensing only	Lensing + CMB
$\Omega_b h^2$	$\mathcal{N}(0.0222, 0.0005^2)$	$\mathcal{U}(0.005, 0.1)$
$\Omega_c h^2$	$\mathcal{U}(0.001, 0.99)$	$\mathcal{U}(0.001, 0.99)$
H_0 [km/s/Mpc]	$\mathcal{U}(40, 100)$	$\mathcal{U}(40, 100)$
τ	0.055	$\mathcal{U}(0.01, 0.8)$
n_s	$\mathcal{N}(0.96, 0.02^2)$	$\mathcal{U}(0.8, 1.2)$
$\ln(10^{10} A_s)$	$\mathcal{U}(1.61, 3.91)$	$\mathcal{U}(1.61, 3.91)$
$\sum m_\nu$ [eV]	0.06	0.06 or $\mathcal{U}(0, 5)$
Ω_K	0	0 or $\mathcal{U}(-0.3, 0.3)$
A_L	1	1 or $\mathcal{U}(0, 10)$
$A_L^{\phi\phi}$	1	1 or $\mathcal{U}(0, 10)$

In particular, we focus on the amplitude of the matter power spectrum σ_8 and the total matter density Ω_m. When analyzing constraints from CMB lensing alone, we follow Planck Collaboration et al. (2018b) and adopt the weak priors shown in Tab. 1 to avoid marginalizing over unrealistic values of poorly constrained parameters. Specifically, we fix the optical depth to reionization to $\tau = 0.055$ and place Gaussian priors on the baryon density $\Omega_b h^2 = 0.0222 \pm 0.0005$, motivated by primordial deuterium abundance D/H measurements in high-redshift metal-poor quasar absorption systems (Cooke et al. 2018) combined with big-bang nucleosynthesis predictions, and on the spectral index $n_s = 0.96 \pm 0.02$. Moreover, we fix the linear corrections to the response function to the fiducial cosmology, similar to Planck Collaboration et al. (2016c); Sherwin et al. (2017); Simard et al. (2018).

As shown in Fig. 3, the lensing-only constraints project a well-defined band in the $\Omega_m - \sigma_8$ plane:

$$\sigma_8 \Omega_m^{0.25} = 0.593 \pm 0.025 \quad (\text{SPTpol lensing only, } 68\%). \tag{13}$$

This parameter combination is measured with a 4.2% precision and is in excellent agreement with the *Planck* lensing-only value of $\sigma_8 \Omega_m^{0.25} = 0.590 \pm 0.020$ (3.4% precision). For comparison, in Fig. 3 we also show the constraints obtained by Simard et al. (2018) with the CMB lensing band powers from 2500 deg^2 observed by SPT-SZ + *Planck* (Omori et al. 2017), which are again consistent with the SPTpol ones and similar in extent.

Assuming that the SPTpol and *Planck* lensing measurements are independent, which is a safe assumption

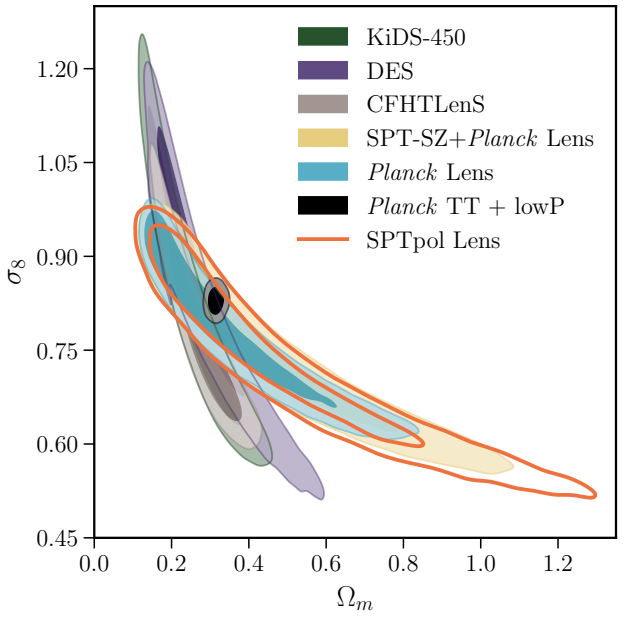


Figure 3. The constraints on σ_8 and Ω_m from CMB lensing (SPTpol, *Planck*, SPT-SZ +*Planck*) and optical lensing (KiDS-450, CFHTLenS, DES) surveys appear to be broadly consistent with each other. The different degeneracy direction between CMB and optical lensing surveys reflects their different redshift sensitivity to matter fluctuations. The independent high-redshift constraints from *Planck* primary CMB power spectra, shown as black contours, are also in agreement with the lower redshift CMB lensing measurements.

given the relatively small footprint overlap and the different sensitivity to CMB modes due to noise and resolution, we can further combine the datasets. The parameter that mostly benefits from the joint analysis is once again $\sigma_8 \Omega_m^{0.25}$, which is constrained with an accuracy of $\approx 2.5\%$:

$$\sigma_8 \Omega_m^{0.25} = 0.587 \pm 0.015 \quad (\textit{Planck} + \text{SPTpol lensing only, } 68\%). \tag{14}$$

This corresponds to a factor of 1.33 improvement over *Planck* lensing-only statistical uncertainties.

3.3. *Comparison with galaxy lensing*

While the focus of this analysis is interpreting the gravitational lensing measurements of the CMB, we are also able to compare our results with measurements of optical weak lensing, also known as cosmic shear (e.g., Bartelmann & Schneider 2001). Cosmic shear is complementary to CMB lensing as it is sensitive to the evolution of gravitational potentials at lower redshift and is affected by different systematics.

In Fig. 3 we also show a compilation of recent cosmic shear constraints on Ω_m and σ_8 from the KiDS[7] (Hildebrandt et al. 2017), CFHTLenS[8] (Joudaki et al. 2017a), and DES (Troxel et al. 2018) optical surveys. We follow the Planck Collaboration et al. (2018b) approach and use the first-year DES cosmic shear likelihood, data cuts, and nuisance parameters (and associated priors) described by Troxel et al. (2018), but use the priors on cosmological parameters shown in Tab 1. Furthermore, we consider a single minimal-mass neutrino eigenstate.

As can be seen in Fig. 3, the statistical power of galaxy lensing constraints is comparable to that of CMB lensing, but due to the much lower redshift distribution of the source galaxies, the degeneracy direction is different and approximately constrains $\sigma_8\Omega_m^{0.5}$. In fact, the parameter combination that is best constrained by cosmic shear measurements is $S_8 = \sigma_8\sqrt{\Omega_m/0.3}$, which is measured at 5% accuracy by DES lensing, $S_8 = 0.790^{+0.040}_{-0.029}$. This constraint is $\sim 1.1\,\sigma$ lower than the value inferred from *Planck* 2018 primary CMB, $S_8 = 0.834 \pm 0.016$, and consistent with S_8 from SPTpol lensing, $S_8 = 0.86 \pm 0.11$. A similar level of precision has been achieved by Hikage et al. (2019) who performed a tomographic analysis of the Hyper Suprime-Cam (HSC) survey first-year shear catalog and found $S_8 = 0.777^{+0.031}_{-0.034}$.[9]

3.4. *Including BAO information*

We next consider the cosmological implication of adding BAO data to the lensing measurements. In addition to σ_8 and Ω_m, the lensing spectrum is sensitive to the expansion rate H_0 since it also constrains the parameter combination $\sigma_8\Omega_m^{0.25}(\Omega_m h^2)^{-0.37}$ (e.g. Planck Collaboration et al. 2016c). To break the degeneracy, we include BAO measurements (and the Gaussian prior on $\Omega_b h^2$ from the column "Lensing only" in Tab. 1), which allow the BAO measurements to constrain H_0 and Ω_m.

[7] We make use of the `kids450fiducial` chains available at https://github.com/sjoudaki/kids450.

[8] Results shown here are based on the `fiducialrun` chains available at https://www.dropbox.com/s/lku48ron59nvc1m/centralchains.tar.gz?dl=0.

[9] For consistency with the results based on CMB lensing and DES cosmic shear, here we quote the constraint obtained by fixing the sum of the neutrino masses to $\sum m_\nu = 0.06$ eV.

Combining SPTpol lensing with BAO, we obtain the following ΛCDM constraints (68%):

$$\left.\begin{aligned} H_0 &= 72.0^{+2.1}_{-2.5}\,\mathrm{km\,s^{-1}\,Mpc^{-1}} \\ \sigma_8 &= 0.779 \pm 0.023 \\ \Omega_m &= 0.368^{+0.032}_{-0.037} \end{aligned}\right\} \text{SPTpol lensing + BAO}, \tag{15}$$

while combining *Planck* lensing with BAO yields:

$$\left.\begin{aligned} H_0 &= 67.9^{+1.1}_{-1.3}\,\mathrm{km\,s^{-1}\,Mpc^{-1}} \\ \sigma_8 &= 0.811 \pm 0.019 \\ \Omega_m &= 0.303^{+0.016}_{-0.018} \end{aligned}\right\} \textit{Planck} \text{ lensing + BAO}. \tag{16}$$

A summary of the constraints from CMB lensing, both *Planck* and SPTpol datasets, and BAO data is provided in Tab. 2. In Fig. 4 we show the constraints on $\Omega_m h^2$, σ_8, and $\ln(10^{10}A_s)$ obtained with SPTpol lensing + BAO (red contours) and *Planck* lensing + BAO (blue contours). The SPTpol + BAO set prefers higher H_0 and Ω_m than the *Planck* + BAO set. Since the included BAO measurements are the same for both cases, the differences in the best-fit parameters are indicative of the different preferences of the two sets of lensing band powers.

To understand the parameter preferences from the two experiments, we first note that H_0 and Ω_m correlate positively in the posterior distribution of the BAO measurements with priors on $\Omega_b h^2$ (e.g., Addison et al. 2018). As discussed in Planck Collaboration et al. (2016c), the shape of the *Planck* lensing spectrum constrains $\Omega_m^{0.6}h \approx$ constant, preferring an anti-correlation between H_0 and Ω_m and thus breaking degeneracies of these parameters. The BAO+$\Omega_b h^2$ constraints dominate the H_0-Ω_m degeneracy direction when combined with SPTpol CMB lensing. Therefore the preference for higher H_0 from SPTpol lensing when combined with BAO is driven by the SPTpol lensing H_0-Ω_m contours intersecting the BAO H_0-Ω_m contours around larger values of H_0 and Ω_m compared to *Planck* lensing. Compared to the *Planck* lensing measurement, SPTpol lensing does not measure the peak of the lensing spectrum. The peak of the lensing spectrum is sensitive to the scale of matter-radiation equality and effectively constrains the matter density $\Omega_m h^2$. Without measurements of the peak, the SPTpol lensing measurement allows for a broader degeneracy between $\Omega_m h^2$ and A_s. Indeed, the best-fit $\Omega_m h^2$ and $\ln(10^{10}A_s)$ from the SPTpol lensing measurement are $\sim 1\sigma$ higher and $\sim 1.4\sigma$ lower compared to the best fits of *Planck*'s lensing measurements. With this preference for a high $\Omega_m h^2$ from the SPTpol lensing spectrum, the constraints on H_0 and Ω_m when com-

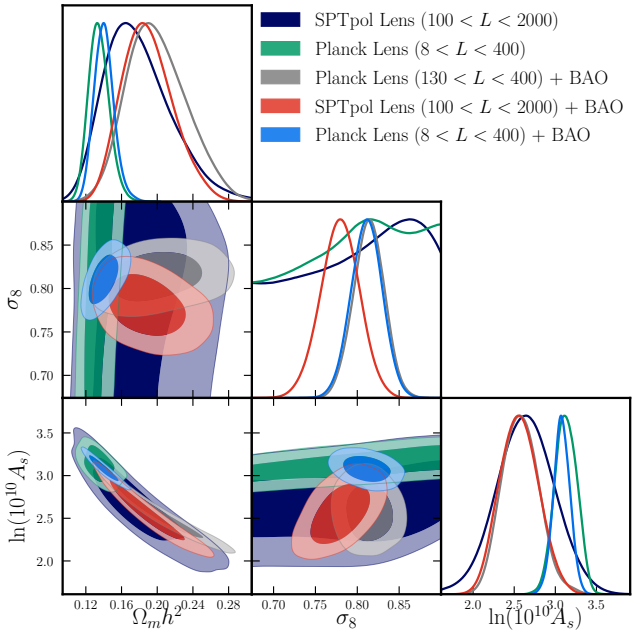


Figure 4. Constraints within the ΛCDM model on $\Omega_m h^2$, σ_8, $\ln(10^{10}A_s)$ from CMB lensing alone and in combination with BAO measurements. We also show the effect of discarding the information about the peak of the CMB lensing power spectrum on the parameter degeneracies (see *Planck* lensing $130 < L < 400$ + BAO). Contours contain 68% and 95% of the posteriors.

bined with BAO are driven high compared to *Planck* lensing.

To confirm this intuition, we rerun the *Planck* lensing + BAO chain discarding the first three band powers covering the peak of the lensing power spectrum. This leaves us with six band powers between $135 < L < 400$ for a naive $S/N \sim \sqrt{\sum_L (C_L^{\phi\phi}/\Delta C_L^{\phi\phi})^2} \sim 25$ (for comparison, SPTpol gives us $S/N \sim 18$). As expected, we find that removing the information about the peak of $C_L^{\phi\phi}$ results in a broadening of the $A_s - \Omega_m h^2$ degeneracy and the contours overlap with the SPTpol ones, see Fig. 4. Specifically, we find the following constraints

$$\left.\begin{array}{l} H_0 = 72.6^{+2.3}_{-2.9}\ \text{km s}^{-1}\ \text{Mpc}^{-1} \\ \sigma_8 \ = 0.814 \pm 0.019 \\ \Omega_m = 0.379^{+0.036}_{-0.042} \end{array}\right\} \begin{array}{l} \textit{Planck}\ \text{lensing} \\ 135 < L < 400 + \text{BAO}\ , \end{array} \tag{17}$$

in agreement with SPTpol lensing + BAO. Recall that our SPTpol CMB lensing + BAO constraints are more sensitive to the low-redshift ($z \lesssim 4$) universe compared to the primary CMB. It is then interesting to compare the constraints on H_0 from CMB lensing + BAO to values inferred from the primary CMB and to direct measurements H_0.

Table 2. Constraints on a subset of ΛCDM parameters using the *Planck* and SPTpol CMB lensing datasets alone, jointly analyzed, or combined with BAO information. All limits in this table are 68% intervals, H_0 is in units of km $\text{s}^{-1}\text{Mpc}^{-1}$.

	Lensing	Lensing + BAO		
	$\sigma_8\Omega_m^{0.25}$	σ_8	H_0	Ω_m
SPTpol	0.593 ± 0.025	0.779 ± 0.023	$72.0^{+2.1}_{-2.5}$	$0.368^{+0.032}_{-0.037}$
Planck	0.590 ± 0.020	0.811 ± 0.019	$67.9^{+1.1}_{-1.3}$	$0.303^{+0.016}_{-0.018}$

Given the degeneracy between the H_0 and Ω_m from the BAO data and the preference for high Ω_m of SPTpol lensing data, the best-fit H_0 from SPTpol lensing + BAO is $72.0^{+2.1}_{-2.5}$ km s^{-1} Mpc^{-1}. This sits between the supernovae and strong gravitational lensing time-delay H_0 values from SH0ES/H0LiCOW (Riess et al. 2019; Wong et al. 2019) and the supernovae based CCHP H_0 values (Freedman et al. 2019), and is within $\sim 1\,\sigma$ of both measurements. Compared to that inferred from *Planck*'s primary CMB spectra (67.27 ± 0.60, Planck Collaboration et al. 2018a, TT+TE+EE+lowE), the SPTpol lensing + BAO H_0 value is also $\sim 2\,\sigma$ high.[10] Note however, the H_0 value depends on the L range of the data, as discussed earlier. This CMB lensing measurement, when combined with BAO + $\Omega_b h^2$ prior, provides a separate inference on H_0 utilizing information from the low-redshift universe.

Let us now look at the constraint on the σ_8 parameter. The value of the amplitude of matter fluctuations suggested by SPTpol + BAO is $\sigma_8 = 0.779 \pm 0.023$. This is consistent, at the $1.1\,\sigma$ level, with the full-sky *Planck* lensing result of $\sigma_8 = 0.811 \pm 0.019$ and $1.8\,\sigma$ lower than the primary CMB result of $\sigma_8 = 0.829 \pm 0.015$. The SPTpol + BAO preference for a lower σ_8 simply represents another way of stating the preference for a lower A_s. Interestingly, as also alluded in Sec. 3.3, there are indications that the σ_8 value inferred from LSS probes such as clusters (e.g., de Haan et al. 2016; Bocquet et al. 2019), cosmic shear (e.g., Hildebrandt et al. 2017; Joudaki et al. 2017a,b; Planck Collaboration et al. 2018b; Abbott et al. 2018; Hikage et al. 2019), and redshift space distortions (e.g., Gil-Marín et al. 2017), are lower than what *Planck* would suggest, although the difference is not as significant as the H_0 tension.

[10] We also note that, thanks to the $H_0 - \Omega_m$ degeneracy in the CMB lensing + BAO data case, the matter density value Ω_m inferred from SPTpol lensing + BAO data is similarly larger, at the $\sim 1.5\,\sigma$ level, than the one suggested by primary CMB (0.3166 ± 0.0084, Planck Collaboration et al. 2018a, TT+TE+EE+lowE).

3.5. *Joint constraints from primary CMB power spectrum and lensing*

Adding primary CMB anisotropy information constrains the angular acoustic scale θ_* to high precision and, in turn, breaks the degeneracy between Ω_m, σ_8, and H_0 that affects the CMB lensing-only constraints. Conversely, CMB lensing data can improve constraints on the amplitude parameters, for example by breaking the $A_s e^{-2\tau}$ degeneracy through lensing smoothing effects, and on those limited by geometrical degeneracies when measured from primary CMB alone.

The joint constraints on Ω_m and σ_8 from the combination of *Planck* primary CMB and CMB lensing data are shown in Fig. 5. Note that in this case, we use the priors shown in the right column of Tab. 1 and apply both the response function and $N_L^{(1)}$ linear corrections to the lensing likelihood, as discussed in Sec. 2.4. When primary CMB data are included, the lensing power spectrum shape is almost fixed, but the amplitude still has freedom to increase (decrease) because matter density is allowed to increase (decrease) through the acoustic-scale degeneracy in the primary CMB. CMB lensing data, either from SPTpol or *Planck*, tend to pull down the σ_8 value inferred from *Planck* primary CMB, as also hinted by Fig. 3. In particular, we find $\sigma_8 = 0.829 \pm 0.015$ from primary CMB alone (PlanckTT + lowP, 68%) and $\sigma_8 = 0.816 \pm 0.012$ (PlanckTT + lowP + SPTpol lensing, 68%) and $\sigma_8 = 0.820 \pm 0.010$ (PlanckTT + lowP + *Planck* lensing, 68%). For completeness, we note that that the σ_8 value inferred from *Planck* 2018 primary CMB data alone reduces to $\sigma_8 = 0.812 \pm 0.009$ (2018 Planck TT+lowE, Planck Collaboration et al. 2018a), thanks to a more precise and lower value of the optical depth, as mentioned in Sec. 3.1. Finally, we note that the geometrical information from BAO further improves constraints on Ω_m by roughly 40% for all datasets considered.

3.6. *Lensing amplitudes*

Gravitational lensing is responsible for transferring CMB power from large to small scales and for smearing the acoustic peaks. Both these effects have been accurately observed and measured in CMB power spectra (e.g., Reichardt et al. 2009; Story et al. 2013; Louis et al. 2017; Henning et al. 2018; Planck Collaboration et al. 2018a).

A well-known internal tension in *Planck* is the preference (at $\approx 2.5\sigma$ significance) of a slightly larger amount of lensing as measured from the smoothing of the acoustic peaks, than what is predicted given ΛCDM (Planck Collaboration et al. 2016b, 2018a). At the same time, we note that similar analyses of the SPT CMB temperature

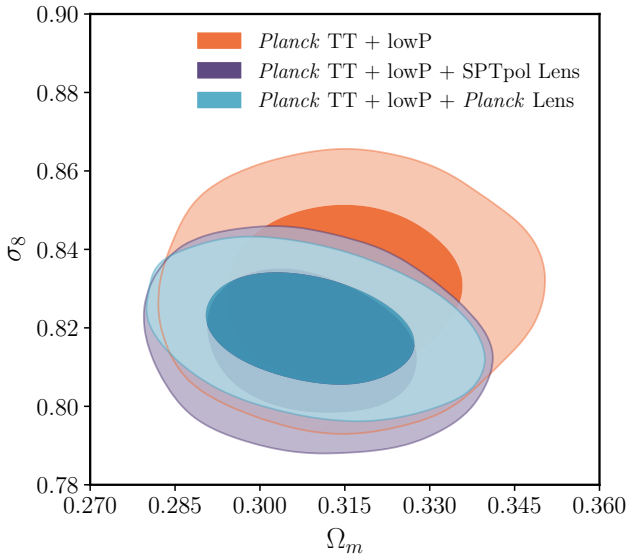


Figure 5. Constraints on Ω_m and σ_8 in the base ΛCDM model from *Planck* primary CMB alone (orange contours) and in combination with *Planck* and SPTpol CMB lensing data (blue and purple contours respectively). Contours contain 68 % and 95 % of the posteriors.

(Story et al. 2013; Aylor et al. 2017) and polarization (Henning et al. 2018) spectra have found no evidence of this enhanced peak smoothing effect, reporting a mild preference ($\approx 1\sigma$) for a lower lensing power than predicted.[11]

The CMB lensing measurement from W19 represents an independent cross-check on the *Planck* lensing amplitude measurement. To this end, we follow Planck Collaboration et al. (2018b); Simard et al. (2018) and introduce two phenomenologically motivated lensing amplitude parameters, A_L and $A_L^{\phi\phi}$. The former is an unphysical parameter that scales the lensing power spectrum both in the acoustic peak smearing and the lens reconstruction, while the latter only scales the theory lens reconstruction at every point in the parameter space.

Marginalizing over A_L effectively removes the lensing information from extra peak-smoothing beyond ΛCDM in the PlanckTT 2-point function. Then, when both parameters are allowed to vary, the combination $A_L \times A_L^{\phi\phi}$ quantifies the overall amplitude of the measured lensing power with respect to ΛCDM expectations, when the inferred ΛCDM parameters are insensitive to the observed level of peak smearing.

[11] The significance of the SPT data preference for low lensing power when compared to *Planck* can be exacerbated if super-sample and intra-sample lensing covariances are neglected, see Motloch & Hu (2019).

We start the comparison between *Planck* and SPTpol lensing by fixing A_L to unity. The preference for $A_L > 1$ in *Planck* temperature data pulls the cosmological parameters to a region of the parameter space with a higher intrinsic CMB lensing power spectrum. This, in turns, leads the inferred lensing amplitude $A_L^{\phi\phi}$ to lower values. Specifically, we find:

$$A_L^{\phi\phi} = 0.890^{+0.057}_{-0.066} \quad \text{SPTpol Lensing, 68\%}, \quad (18)$$

$$A_L^{\phi\phi} = 0.970 \pm 0.039 \quad \textit{Planck} \text{ Lensing, 68\%}, \quad (19)$$

both in combination with PlanckTT and lowP. As can be seen, *Planck* lensing is consistent within 1σ to the ΛCDM expectations based on *Planck* primary CMB, while the SPTpol measurement is about 1.8σ lower than $A_L^{\phi\phi} = 1$. Note that the SPTpol-based $A_L^{\phi\phi}$ value quoted here (Eq. 18) differs from $A_L^{\phi\phi} = 0.944 \pm 0.058$ (stat) reported in W19 because here we marginalize over the six ΛCDM cosmological parameters. An indication of a mild lensing power deficit was also seen in the SPT-SZ + *Planck* lensing measurement from Omori et al. (2017), for which Simard et al. (2018) estimate $A_L^{\phi\phi} = 0.91 \pm 0.06$, consistent with both the SPTpol and *Planck* values presented here.

An informative check to perform is replacing PlanckTT with the SPTpol TEEE dataset. This way we can test the impact of primary CMB on the inferred lensing power spectrum amplitude. As expected, the mild SPTpol preference for less lensing smoothing pushes the inferred 4-point lensing amplitude to values $\approx 1\sigma$ above unity:

$$A_L^{\phi\phi} = 1.13^{+0.13}_{-0.11} \quad \text{SPTpol Lensing, 68\%}. \quad (20)$$

The constraints on $A_L^{\phi\phi}$ from different combinations of datasets are reported in Tab. 3.

The next question we would like to answer is whether the lensing power observed in the 4-point function is consistent with ΛCDM expectations when the peak smoothing effect, from either *Planck* or SPTpol primary CMB, is not reflected on the cosmological constraints. To investigate this aspect, we show in Fig. 6 the posterior distributions on A_L and $A_L \times A_L^{\phi\phi}$ using *Planck* primary CMB in combination with *Planck* and SPTpol lensing datasets (purple and orange contours respectively). When letting both A_L and $A_L^{\phi\phi}$ free to vary, we obtain (with PlanckTT and lowP, 68%)

$$A_L \times A_L^{\phi\phi} = 0.995 \pm 0.090 \quad \text{SPTpol Lensing}, \quad (21)$$

$$A_L \times A_L^{\phi\phi} = 1.076 \pm 0.063 \quad \textit{Planck} \text{ Lensing}, \quad (22)$$

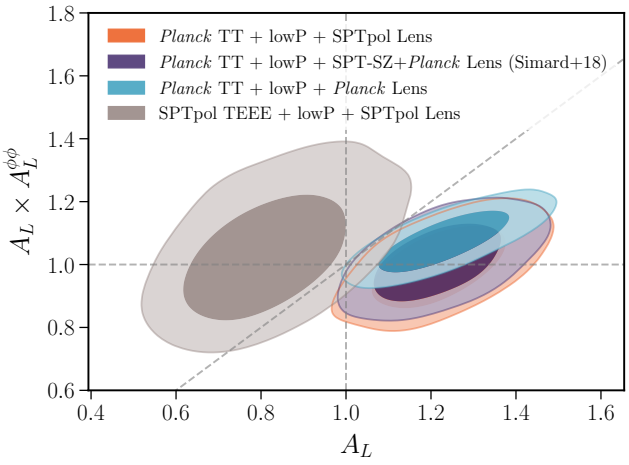


Figure 6. The CMB lensing and primary CMB power spectra are sensitive to the lensing effects in different ways. The acoustic peak smoothing induced by lensing on *Planck* primary CMB favours models with $A_L > 1$. When the peak smearing information has been marginalized over, the amplitude of the lensing trispectrum relative to the best-fit ΛCDM parameters is consistent with expectations independent of the dataset combination. The results based on the SPT-SZ + *Planck* lensing map from Omori et al. (2017) presented in Simard et al. (2018) are also consistent with the SPTpol constraints.

These values show that both lensing datasets appear consistent with the cosmological parameters implied by the 2-point function, once peak-smearing effects are marginalized over. Finally, the SPTpol lensing dataset is also consistent with ΛCDM expectations when *Planck* primary CMB is replaced with SPTpol *TEEE*, with information from peak smoothing marginalized over:

$$A_L \times A_L^{\phi\phi} = 1.036 \pm 0.136 \quad \text{SPTpol Lensing, 68\%}. \quad (23)$$

The individual constraints on A_L and $A_L^{\phi\phi}$ when both are allowed to vary are summarized in Tab. 3. Note how both *Planck* and SPTpol preferences for $A_L \neq 1$ are preserved even when $A_L^{\phi\phi}$ is included as an additional parameter. This demonstrates that the driver of A_L best-fit values is the features in both the *Planck* and SPTpol 2-point CMB spectra.

3.7. *Massive neutrinos*

We now turn to examine what CMB lensing measurements tell us about fundamental physics, specifically about neutrino properties. Despite the fact that neutrino oscillation measurements have established that neutrinos are massive, their absolute mass scale and the relative ordering of the mass eigenstates - the so-called neutrino hierarchy - are still largely unknown. Neutrino

oscillation experiments are sensitive to the squared mass differences and suggest that the sum of the neutrino masses is $\sum m_\nu > 58$ meV in the normal hierarchy and > 100 meV in the inverted hierarchy (de Salas et al. 2017, and references therein). Interestingly, the current generation of long baseline neutrino oscillation experiments such as T2K[12] and NOνA[13], which are mostly sensitive to the mass hierarchy, have found a mild preference for the normal hierarchy (Abe et al. 2017; Acero et al. 2019).

In the context of neutrino studies, cosmological observations greatly complement laboratory measurements as they enable a constraint of the sum of the neutrino masses (e.g., Vagnozzi et al. 2017). In particular, the CMB lensing potential power spectrum is sensitive to $\sum m_\nu$ since massive neutrinos suppress the growth of structure below the neutrino free-streaming length, resulting in a scale-dependent suppression of $C_L^{\phi\phi}$.

Let us first look at the constraints on $\sum m_\nu$ from primary CMB alone. *Planck* constrains the sum of the neutrino masses to $\sum m_\nu < 0.69$ eV at 95% level (PlanckTT + lowP). This upper limit can be further improved by adding data on the BAO scale, as the low-redshift information allows us to break parameter degeneracies, for instance between $\sum m_\nu$ and H_0. With this setup, we obtain $\sum m_\nu < 0.20$ eV (95%), which is shown by the black solid line in Fig. 7 (for the remainder of this subsection we always include BAO data unless otherwise stated). As mentioned in Sec. 3.6, the amount of lensing inferred from primary CMB is larger than the one directly measured through the amplitude of the lensing power spectrum. Therefore, the constraints on $\sum m_\nu$ from primary CMB alone (+BAO) are tighter when CMB lensing is not included. This is because increasing the neutrino mass corresponds to a decrease in the acoustic peak smearing expected within ΛCDM.

In fact, after the inclusion of CMB lensing information we obtain:

$$\sum m_\nu < 0.23\,\text{eV} \quad (\text{PlanckTT + lowP + BAO} \\ \text{+SPTpol lensing, 95\%}), \tag{24}$$

$$\sum m_\nu < 0.22\,\text{eV} \quad (\text{PlanckTT + lowP + BAO} \\ \text{+}\textit{Planck}\text{ lensing, 95\%}), \tag{25}$$

[12] https://t2k-experiment.org/
[13] https://novaexperiment.fnal.gov/

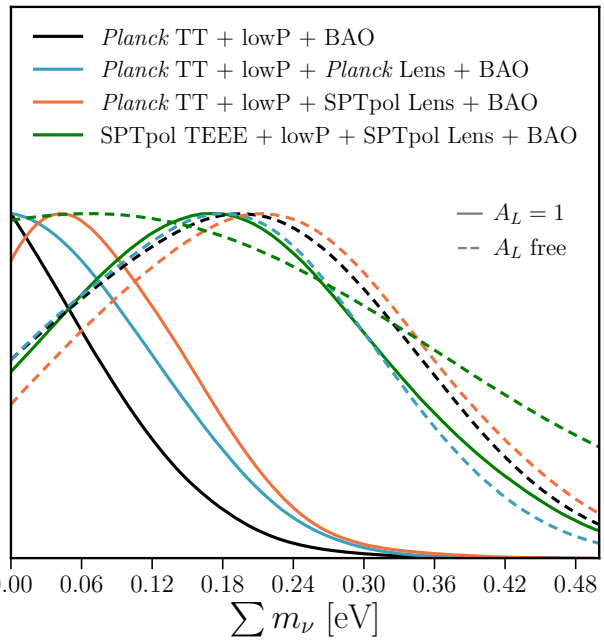


Figure 7. Constraints on the sum of the neutrino masses $\sum m_\nu$ when *Planck* primary CMB and BAO information is exploited (black line) and when either SPTpol lensing (orange line) or *Planck* lensing (cyan line) is included in the cosmological analysis. If we replace the *Planck* primary CMB with the SPTpol TEEE measurement from Henning et al. (2018) and include SPTpol lensing and BAO we obtain the green curve. Dashed lines show instead the results when we marginalize over the lensing information in the primary CMB, i.e. we let A_L free to vary.

shown as the solid orange and cyan lines in Fig. 7. These results are in good agreement with each other. For a direct comparison with the previous SPT-SZ lensing measurement, Simard et al. (2018) find a 95% upper limit on the sum of the neutrino masses of $\sum m_\nu < 0.70$ eV, while we obtain $\sum m_\nu < 0.72$ eV when replacing SPT-SZ +*Planck* lensing with SPTpol lensing, both without BAO.

An instructive test to check the stability of the neutrino mass constraints with respect to changes in the primary CMB is replacing the PlanckTT likelihood with the SPTpol TEEE one from Henning et al. (2018). This test is especially interesting because, as we have already mentioned, the *Planck* and SPTpol primary CMB measurements are known to favour different amount of lensing from the smoothing of the acoustic

peaks. In fact, this dataset combination (the solid green line in Fig. 7) suggests

$$\sum m_\nu < 0.42\,\mathrm{eV} \quad (\text{SPTpol TEEE + lowP + BAO +SPTpol lensing, 95\%}), \tag{26}$$

which is larger than what is found using the temperature and large scale polarization from *Planck*. Differently from PlanckTT measurement, the high-ℓ SPTpol TEEE spectra prefer slightly less lensing than in base ΛCDM ($1.4\,\sigma$ below $A_L = 1.0$ and $2.9\,\sigma$ lower than the value preferred by PlanckTT). In turn, the lensing power deficit is interpreted as a larger neutrino mass due to their structure suppression effect, pushing the constraints on $\sum m_\nu$ to larger values.

Finally, we free the lensing amplitude parameter A_L and investigate the SPTpol lensing constraining power when we marginalize over the effect on $\sum m_\nu$ from excess peak smoothing of the primary *Planck* 2-point measurements. This is particularly interesting in light of *Planck*'s A_L being $2.5\,\sigma$ high compared to ΛCDM expectation (Planck Collaboration et al. 2018a). The results are shown as the dashed lines in Fig. 7 with the same color coding introduced above.

When using PlanckTT as the primary CMB, A_L takes on values greater than 1 due to the significant constraining power of the 2-point power spectrum. This, compared to when A_L is fixed to 1, lets the matter parameters take on lower values and allows for a larger value of $\sum m_\nu$. As a result, the 95% C.L. upper limits on $\sum m_\nu$ from both *Planck* lensing and SPTpol lensing increase to:

$$\sum m_\nu < 0.45\,\mathrm{eV} \quad (\text{PlanckTT + lowP + BAO +SPTpol lensing } [A_L \text{ free}],\ 95\%), \tag{27}$$

$$\sum m_\nu < 0.39\,\mathrm{eV} \quad (\text{PlanckTT + lowP + BAO +}\textit{Planck}\text{ lensing } [A_L \text{ free}],\ 95\%). \tag{28}$$

As can be noted from Tab. 3, when CMB lensing likelihood is included in the cosmological inference, the central value of A_L is still larger than unity (e.g., $A_L = 1.15^{+0.09}_{-0.12}$ for SPTpol lensing), while for primary CMB + BAO we find $A_L = 1.28^{+0.10}_{-0.13}$.

On the other hand, when using the SPTpol *TEEE* measurement instead of PlanckTT, A_L, instead of having a $1.4\,\sigma$ lower value as would be preferred by SPTpol TEEE, takes on the value $A_L = 1.03^{+0.28}_{-0.23}$. Thus the best-fit posterior values in this A_L-free chain are similar to the $A_L = 1$ chain. However, since $\sum m_\nu$ and A_L are degenerate (positively correlated), including A_L as a free parameter essentially broadens the posterior distribution of $\sum m_\nu$. Therefore, we obtain a larger upper limit on $\sum m_\nu$, specifically we find:

$$\sum m_\nu < 0.62\,\mathrm{eV} \quad (\text{SPTpol TEEE + lowP + BAO +SPTpol lensing } [A_L \text{ free}],\ 95\%). \tag{29}$$

The constraint on the sum of neutrino masses from SPTpol lensing is consistent with *Planck* lensing, allowing slightly higher neutrino mass because of the overall smaller lensing amplitude.

3.8. *Spatial curvature*

A general prediction of inflationary models is the flatness of the spatial hyper-surfaces of the background metric. A main hindrance in determining the geometry of the universe solely from primary CMB observations is the well-known geometrical degeneracy (Efstathiou & Bond 1999). This degeneracy arises because the shape of the CMB anisotropy spectrum mainly depends on two physical scales, the sound horizon at recombination and the angular diameter distance to the last scattering surface, so that cosmological models with similar matter content and angular diameter distance to the last scattering surface will produce nearly indistinguishable CMB power spectra.

The geometrical degeneracy is manifest when looking at the coloured scattered points in Fig. 8 that have been obtained using only *Planck* primary CMB data. In particular, the PlanckTT preference for larger A_L values allows the degeneracy to extend to regions of the parameter space with low Hubble constant and negative curvature. This picture can be greatly improved by using either internal CMB data alone, specifically by adding measurements of CMB lensing that break the geometrical degeneracy, or through the inclusion of BAO data. The constraint on spatial curvature from *Planck* primary CMB only is $\Omega_K = -0.043^{+0.028}_{-0.016}$, favouring a positive curvature at about $1.5\,\sigma$. Instead, the inclusion of SPTpol CMB lensing yields

$$\Omega_K = -0.0099^{+0.013}_{-0.0084} \quad (\text{PlanckTT + lowP +SPTpol lensing, 68\%}) \tag{30}$$

in agreement with the *Planck* lensing based result of $\Omega_K = -0.0084^{+0.0093}_{-0.0076}$.

Table 3. Constraints on several extensions to the base six parameters ΛCDM model for combinations of primary CMB and lensing power spectra from *Planck* and SPTpol. Horizontal lines separate the different cosmological models that have been analyzed. All limits are 68% except on $\sum m_\nu$, for which we report the 95% upper limits. Note that the results for cosmological runs with varying $\sum m_\nu$ also include BAO information in addition to the datasets shown in the first row. The number in parenthesis in the Ω_K run also shows the effect of the BAO data inclusion.

	TT + lowP	TT + lowP + SPTpol Lens	TT + lowP + *Planck* Lens	SPTpol TEEE + lowP + SPTpol Lens
$A_L^{\phi\phi}$	...	$0.890^{+0.057}_{-0.066}$	0.970 ± 0.039	$1.13^{+0.11}_{-0.13}$
$A_L^{\phi\phi}$	...	0.817 ± 0.065	$0.876^{+0.042}_{-0.052}$	$1.27^{+0.15}_{-0.21}$
A_L	...	$1.222^{+0.097}_{-0.11}$	$1.233^{+0.093}_{-0.11}$	$0.70^{+0.15}_{-0.20}$
$A_L \times A_L^{\phi\phi}$	...	0.995 ± 0.090	1.076 ± 0.063	1.036 ± 0.136
$\sum m_\nu$ [eV]	<0.196	<0.229	<0.223	<0.420
$\sum m_\nu$ [eV]	<0.430	<0.453	<0.394	<0.620
A_L	$1.28^{+0.10}_{-0.13}$	$1.15^{+0.09}_{-0.12}$	$1.11^{+0.07}_{-0.08}$	$1.03^{+0.09}_{-0.15}$
Ω_K	$-0.050^{+0.030}_{-0.017}$ (0.0005 ± 0.0026)	$-0.0099^{+0.013}_{-0.0084}$ (0.0007 ± 0.0025)	$-0.0084^{+0.0093}_{-0.0076}$ (0.0002 ± 0.0026)	... ...

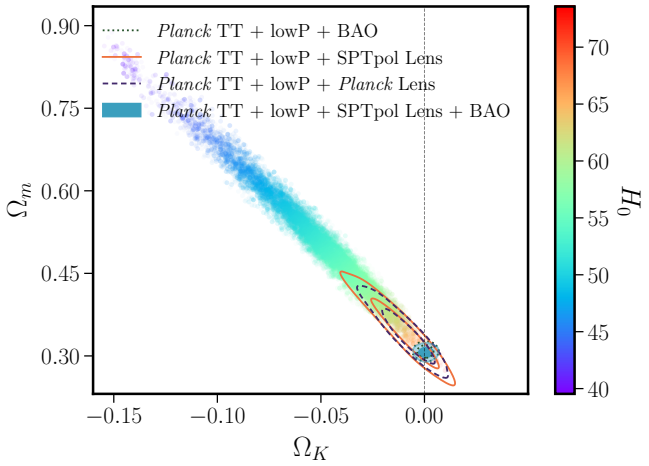


Figure 8. Constraints on curvature and total matter density from primary CMB (scattered points color-coded by Hubble constant value). Closed universe models with high curvature are inconsistent with lensing measurements (solid red and dashed purple lines, SPTpol and *Planck* lensing respectively) and ruled out by BAO data (dotted green line). The joint analysis of *Planck* primary CMB, SPTpol lensing, and BAO is fully consistent with a flat universe (blue shaded contour).

Finally, external data like BAO also provide consistent results when combined with primary CMB *Planck* data (see Fig. 8). By jointly analysing PlanckTT + lowP + SPTpol lensing + BAO we find $\Omega_K = -0.0007 \pm 0.0025$, a sub-percent measurement of the spatial curvature of the universe.

4. CONCLUSIONS

The lensing band powers presented by Wu et al. (2019) are currently the most precise measurement of the CMB lensing power spectrum from the ground. As such, the band powers present a valuable, independent check on the full-sky *Planck* lensing measurement, and also extend the measurement to smaller angular scales. In this work, we investigate the cosmological implications of these data, and explore the tensions that are emerging between the high- and low-redshift universe within the ΛCDM framework.

Overall, the constraints based on SPTpol lensing are in close agreement with the ones obtained on the full-sky with *Planck*. For example, using only SPTpol CMB lensing data, we find a 4.2% constraint on $\sigma_8\Omega_m^{0.25} = 0.593 \pm 0.025$, matching the *Planck* based value of $\sigma_8\Omega_m^{0.25} = 0.590 \pm 0.020$. If we further combine the SPTpol and *Planck* lensing likelihoods, we improve the constraint precision from CMB lensing alone to 2.5%, $\sigma_8\Omega_m^{0.25} = 0.587 \pm 0.015$. When complementing the SPTpol lensing likelihood with BAO data, the constraints tighten to $\sigma_8 = 0.779 \pm 0.023$ and $\Omega_m = 0.368^{+0.032}_{-0.037}$, which when compared to similar constraints using *Planck* lensing with BAO data are $\sim 1.5\,\sigma$ lower and higher, respectively. We identify the lack of information about the peak of the CMB lensing spectrum from the SPTpol data to be the driving factor of this difference.

The SPTpol lensing band powers also provide an informative cross-check on the internal *Planck* tension that exists between the amount of lensing directly measured from the 4-point function reconstruction and the one inferred from the acoustic peak smearing. In particular, the lensing amplitude measured from SPTpol is consistent (albeit $\approx 1\,\sigma$ low) with the one inferred from the *Planck* lensing reconstruction, and in tension with that deduced from CMB peak smearing. When the sensitivity to lensing is removed from the peak smearing effect in the CMB 2-point function, the SPTpol data

match the amount of lensing predicted by the observed primary CMB anisotropies.

When combined with *Planck* primary CMB data, the SPTpol lensing and *Planck* lensing constraints agree. Among the single-parameter extensions to the ΛCDM model that we consider, the spatial curvature is constrained to be $\Omega_K = -0.0007 \pm 0.0025$, while the sum of the neutrino masses $\sum m_\nu < 0.23$ eV at 95% confidence (both including BAO data).

The preference for a larger lensing signal in the *Planck* CMB 2-point function is known to drive tighter constraints on the sum of the neutrino masses (Planck Collaboration et al. 2018a). If we remove the 2-point lensing signal from the PlanckTT peak smearing by marginalizing over A_L, the constraint on $\sum m_\nu$ broadens to $\sum m_\nu < 0.45$ eV. Conversely, when replacing the *Planck* primary CMB with the SPTpol TEEE band powers from Henning et al. (2018), which favour $A_L < 1$, we find $\sum m_\nu < 0.42$ eV (fixing A_L to unity).

The cosmological constraints presented in this paper are also in excellent agreement with those obtained from the SPT-SZ temperature-based lensing reconstruction over 2500 deg^2 (Omori et al. 2017; Simard et al. 2018), of which the SPTpol footprint is a subset.

CMB lensing measurements are becoming increasingly important to precision tests of cosmology. In the upcoming years, high-S/N lensing measurements will provide invaluable insights on the growth of structure and the sum of the neutrino masses. Current experiments like SPT-3G (Benson et al. 2014; Bender et al. 2018), as well as future ground-based observations from Simons Observatory (The Simons Observatory Collaboration et al. 2018) and CMB-S4 (CMB-S4 Collaboration et al. 2016), are projected to significantly improve constraints on the sum of neutrino masses through CMB lensing, with CMB-S4 obtaining a sufficient sensitivity (~ 20 meV[14]) to detect the minimum mass in the normal hierarchy at a significance of $3\,\sigma$. Estimating and removing the CMB lensing signal, a process known as delensing (e.g., Smith et al. 2009; Manzotti et al. 2017), will also be crucial to searches for primordial gravitational waves from inflation. The ultra-low-noise maps of 1500 deg^2 of sky from the on-going SPT-3G survey, the latest instrument on the South Pole Telescope (Benson et al. 2014; Bender et al. 2018), will dramatically improve the lensing reconstruction across this area and our knowledge of high-redshift structure growth.

SPT is supported by the National Science Foundation through grant PLR-1248097. Partial support is also provided by the NSF Physics Frontier Center grant PHY-1125897 to the Kavli Institute of Cosmological Physics at the University of Chicago, the Kavli Foundation and the Gordon and Betty Moore Foundation grant GBMF 947. This research used resources of the National Energy Research Scientific Computing Center (NERSC), a DOE Office of Science User Facility supported by the Office of Science of the U.S. Department of Energy under Contract No. DE-AC02-05CH11231. The Melbourne group acknowledges support from the University of Melbourne and an Australian Research Council's Future Fellowship (FT150100074). Work at Argonne National Lab is supported by UChicago Argonne LLC, Operator of Argonne National Laboratory (Argonne). Argonne, a U.S. Department of Energy Office of Science Laboratory, is operated under contract no. DE-AC02-06CH11357. We also acknowledge support from the Argonne Center for Nanoscale Materials.

[14] Note that this forecast includes projected measurements of the BAO scale from DESI redshift survey.

REFERENCES

Abazajian, K. N., Arnold, K., Austermann, J., et al. 2015, Astroparticle Physics, 63, 66

Abbott, T. M. C., Abdalla, F. B., Alarcon, A., et al. 2018, arXiv e-prints, arXiv:1810.02322

Abe, K., Amey, J., Andreopoulos, C., et al. 2017, PhRvD, 96, 092006

Acero, M. A., Adamson, P., Aliaga, L., et al. 2019, arXiv e-prints, arXiv:1906.04907

Addison, G. E., Watts, D. J., Bennett, C. L., et al. 2018, ApJ, 853, 119

Alam, S., Ata, M., Bailey, S., et al. 2017, MNRAS, 470, 2617

Aylor, K., Hou, Z., Knox, L., et al. 2017, ApJ, 850, 101

Bartelmann, M., & Schneider, P. 2001, PhR, 340, 291

Beck, D., Fabbian, G., & Errard, J. 2018, PhRvD, 98, 043512

Bender, A. N., Ade, P. A. R., Ahmed, Z., et al. 2018, in Society of Photo-Optical Instrumentation Engineers (SPIE) Conference Series, Vol. 10708, Millimeter, Submillimeter, and Far-Infrared Detectors and Instrumentation for Astronomy IX, 1070803

Benson, B. A., Ade, P. A. R., Ahmed, Z., et al. 2014, in Society of Photo-Optical Instrumentation Engineers (SPIE) Conference Series, Vol. 9153, Society of Photo-Optical Instrumentation Engineers (SPIE) Conference Series, 1

Bernardeau, F. 1997, A&A, 324, 15

Beutler, F., Blake, C., Colless, M., et al. 2011, MNRAS, 416, 3017

Blanchard, A., & Schneider, J. 1987, A&A, 184, 1

Bocquet, S., Dietrich, J. P., Schrabback, T., et al. 2019, ApJ, 878, 55

Böhm, V., Schmittfull, M., & Sherwin, B. D. 2016, PhRvD, 94, 043519

CMB-S4 Collaboration, Abazajian, K. N., Adshead, P., et al. 2016, ArXiv e-prints, arXiv:1610.02743

Cooke, R. J., Pettini, M., & Steidel, C. C. 2018, ApJ, 855, 102

Das, S., Sherwin, B. D., Aguirre, P., et al. 2011, Physical Review Letters, 107, 021301

de Haan, T., Benson, B. A., Bleem, L. E., et al. 2016, ApJ, 832, 95

de Salas, P. F., Forero, D. V., Ternes, C. A., Tortola, M., & Valle, J. W. F. 2017, arXiv e-prints, arXiv:1708.01186

Efstathiou, G., & Bond, J. R. 1999, MNRAS, 304, 75

Freedman, W. L., Madore, B. F., Hatt, D., et al. 2019, arXiv e-prints, arXiv:1907.05922

Gil-Marín, H., Percival, W. J., Verde, L., et al. 2017, MNRAS, 465, 1757

Hanson, D., Challinor, A., Efstathiou, G., & Bielewicz, P. 2011, PhRvD, 83, 043005

Hartlap, J., Simon, P., & Schneider, P. 2007, A&A, 464, 399

Henning, J. W., Sayre, J. T., Reichardt, C. L., et al. 2018, ApJ, 852, 97

Hikage, C., Oguri, M., Hamana, T., et al. 2019, PASJ, 71, 43

Hildebrandt, H., Viola, M., Heymans, C., et al. 2017, MNRAS, 465, 1454

Hu, W., & Okamoto, T. 2002, Astrophys.J., 574, 566

Joudaki, S., Blake, C., Heymans, C., et al. 2017a, MNRAS, 465, 2033

Joudaki, S., Mead, A., Blake, C., et al. 2017b, MNRAS, 471, 1259

Joudaki, S., Hildebrandt, H., Traykova, D., et al. 2019, arXiv e-prints, arXiv:1906.09262

Keck Array, T., BICEP2 Collaborations, :, et al. 2016, ArXiv e-prints, arXiv:1606.01968

Kesden, M., Cooray, A., & Kamionkowski, M. 2003, PhRvD, 67, 123507

Lesgourgues, J., & Pastor, S. 2006, PhR, 429, 307

Lewis, A., & Bridle, S. 2002, PhRvD, 66, 103511

Lewis, A., & Challinor, A. 2006, PhR, 429, 1

Lewis, A., Challinor, A., & Lasenby, A. 2000, ApJ, 538, 473

Louis, T., Grace, E., Hasselfield, M., et al. 2017, Journal of Cosmology and Astro-Particle Physics, 2017, 031

Manzotti, A., Story, K. T., Wu, W. L. K., et al. 2017, ApJ, 846, 45

Mead, A. J., Peacock, J. A., Heymans, C., Joudaki, S., & Heavens, A. F. 2015, MNRAS, 454, 1958

Motloch, P., & Hu, W. 2019, PhRvD, 99, 023506

Namikawa, T., Hanson, D., & Takahashi, R. 2013, MNRAS, 431, 609

Omori, Y., Chown, R., Simard, G., et al. 2017, ApJ, 849, 124

Peloton, J., Schmittfull, M., Lewis, A., Carron, J., & Zahn, O. 2017, PhRvD, 95, 043508

Planck Collaboration, Aghanim, N., Arnaud, M., et al. 2016a, A&A, 594, A11

Planck Collaboration, Ade, P. A. R., Aghanim, N., et al. 2016b, A&A, 594, A13

—. 2016c, A&A, 594, A15

Planck Collaboration, Aghanim, N., Akrami, Y., et al. 2018a, arXiv e-prints, arXiv:1807.06209

—. 2018b, arXiv e-prints, arXiv:1807.06210

Planck Collaboration XVII. 2013, A&A, arXiv:1303.5077

POLARBEAR Collaboration. 2014, Phys.Rev.Lett., 113, 021301

Pratten, G., & Lewis, A. 2016, Journal of Cosmology and Astro-Particle Physics, 2016, 047

Reichardt, C. L., Ade, P. A. R., Bock, J. J., et al. 2009, ApJ, 694, 1200

Riess, A. G., Casertano, S., Yuan, W., Macri, L. M., & Scolnic, D. 2019, ApJ, 876, 85

Ross, A. J., Samushia, L., Howlett, C., et al. 2015, MNRAS, 449, 835

Schmittfull, M. M., Challinor, A., Hanson, D., & Lewis, A. 2013, PhRvD, 88, 063012

Sherwin, B. D., van Engelen, A., Sehgal, N., et al. 2017, PhRvD, 95, 123529

Simard, G., Omori, Y., Aylor, K., et al. 2018, ApJ, 860, 137

Smith, K. M., Cooray, A., Das, S., et al. 2009, in American Institute of Physics Conference Series, Vol. 1141, American Institute of Physics Conference Series, 121–178

Stompor, R., & Efstathiou, G. 1999, MNRAS, 302, 735

Story, K. T., Reichardt, C. L., Hou, Z., et al. 2013, ApJ, 779, 86

Story, K. T., Hanson, D., Ade, P. A. R., et al. 2015, ApJ, 810, 50

Takahashi, R., Sato, M., Nishimichi, T., Taruya, A., & Oguri, M. 2012, ApJ, 761, 152

The Simons Observatory Collaboration, Ade, P., Aguirre, J., et al. 2018, ArXiv e-prints, arXiv:1808.07445

Troxel, M. A., MacCrann, N., Zuntz, J., et al. 2018, PhRvD, 98, 043528

Vagnozzi, S., Giusarma, E., Mena, O., et al. 2017, Phys. Rev., D96, 123503

van Engelen, A., Bhattacharya, S., Sehgal, N., et al. 2014, ApJ, 786, 13

van Engelen, A., Keisler, R., Zahn, O., et al. 2012, ApJ, 756, 142

Wong, K. C., Suyu, S. H., Chen, G. C. F., et al. 2019, arXiv e-prints, arXiv:1907.04869

Wu, W. L. K., Mocanu, L. M., Ade, P. A. R., et al. 2019, arXiv e-prints, arXiv:1905.05777

Zaldarriaga, M., & Seljak, U. 1999, PhRvD, 59, 123507

Zubeldia, Í., & Challinor, A. 2019, arXiv e-prints, arXiv:1904.07887